New Sensory Method for Neural Activity by Frequency Upconversion with Non-Linear Element

Chemical and biological sensors

New Sensory Method for Neural Activity by Frequency Upconversion With Nonlinear Element

Andrea Bontempi[1*], Ali Meimandi[2**], Gian Luca Barbruni[2**], Paolo Stefano Crovetti[1***], Danilo Demarchi[1***], Sandro Carrara[2†], and Paolo Motto Ros[1**]

[1]*Department of Electronics, Telecommunications (DET) of Politecnico di Torino, 10129 Torino, Italy*
[2]*Bio/CMOS Interfaces Laboratory (BCI), École Polytechnique Fédérale de Lausanne (EPFL), 2000 Neuchatel, Switzerland*
[*]*Graduate Student Member, IEEE*
[**]*Member, IEEE*
[***]*Senior Member, IEEE*
[†]*Fellow, IEEE*

Manuscript received 26 April 2024; revised 26 June 2024; accepted 12 July 2024. Date of publication 18 July 2024; date of current version 31 July 2024.

Abstract—Traditional analog front-ends for biomedical signal acquisitions operate at very low frequencies (Hz-range) and are severely affected by flicker and environmental noise, which degrade the quality of low-frequency signals, thereby reducing the signal-to-noise ratio (SNR). While offering advantages, the increasingly common use of microelectrodes poses challenges due to their low-frequency high impedance, which is comparable to the one of the front-end, thus creating additional difficulties in signal acquisition. To tackle the challenges of in-vitro low-frequency biosignal acquisition, this letter proposes a novel methodology based on the upconversion of low-frequency biosignals to a higher frequency band by a Schottky diode immersed in a solution. This letter aims to demonstrate the feasibility of the new sensory method by translating in frequency the information of a sinewave stimulus representing a biological signal. Experimental results showed a conversion loss of 11.11 dB and demonstrated the upconverted signal propagation in the solution, measuring an intermodulation power above the noise floor, from −87.04 to −104.13 dBm. The proposed method provides a better signal-to-noise ratio than the traditional acquisition method, estimating an improvement of 8.99 dB.

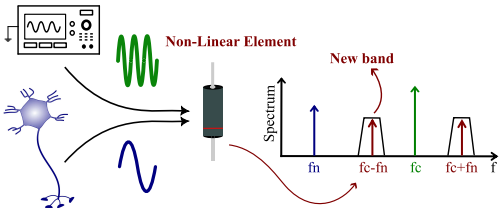

Index Terms—Chemical and biological sensors, biosignal recording, frequency translation, in vitro neural recording, nonlinear mixing product.

I. INTRODUCTION

Acquiring biomedical signals is crucial in medical research, diagnosing, and treating various medical conditions. In vitro acquisitions are useful alternatives to in vivo experiments to study cell pathologies, their interactions, and reactions to medical treatments in a controlled environment [1]. Neural cell cultures are used to study the development of neural connections and neuron interactions [2], neuronal pathologies [3], and to develop new methods for acquiring neural signals (potentiometric and amperometric) [4]. In vitro acquisitions allow both intracellular and extracellular recordings. Extracellular signals include: 1) extracellular action potential (100 Hz to 10 kHz, 50 μV_{pp} 500 μV_{pp}) and 2) local field potential (1 mHz to 200 Hz, 0.5 mV_{pp} to 5 mV_{pp}) [5]. Intracellular recordings are instead characterized by an amplitude ranging from 10 mV_{pp} to 80 mV_{pp}, measured through sharp microelectrodes penetrating the neural membrane. In all the cases, the standard analog front-end to measure neural signals typically includes a low-noise amplifier (LNA) [see Fig. 1(a)].

Despite advancements in LNAs gain, power consumption, and miniaturization [6], [7], neural recordings face several challenges. First, noise is a significant concern, as low-frequency signals are primarily subject to flicker noise ($1/f$) and environmental noise.

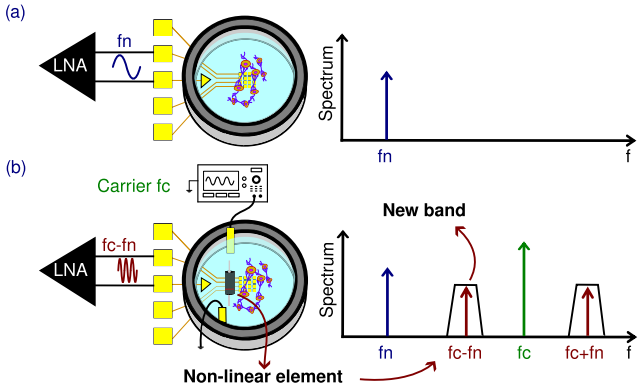

Fig. 1. (a) Classical methodology used for neural recording in vitro. (b) New sensory method for frequency translation of biological signals. The low-frequency biological signal is mixed with a high-frequency carrier and upconverted using a nonlinear element.

Therefore, ultra-low-noise stages are needed to achieve a sufficient signal-to-noise ratio (SNR) while increasing area and power consumption. Second, the microelectrode impedance increases with the reduction of geometrical surface area and as the sampling frequency decreases [8]. Third, the microelectrodes introduce an offset of tens of mV, typically mitigated with a high-pass filter [9]. However, given the low-frequency nature of the biosignal, filtering may not suffice.

Corresponding author: Andrea Bontempi (e-mail: andrea.bontempi@polito.it).
Associate Editor: S.-R. Kothapalli.
Digital Object Identifier 10.1109/LSENS.2024.3430493

This letter presents a new sensory method for measuring and studying biological signals in vitro Fig. 1(b). The idea is to add a passive nonlinear element (e.g., diode) immersed in the solution and inject a high-frequency carrier. The nonlinear element acts like a mixer by upconverting the biosignal information in frequency. The feasibility of the proposed method is discussed based on experimental tests.

II. MATERIAL AND METHOD

The proposed measurement system uses a nonlinear element (diode) to mix a biological/neural signal (f_n) and a high-frequency carrier (f_c). The current flowing in the diode $i_D(t)$ is related to the forward diode voltage $v_D(t)$ as

$$i_D(t) = I_s\left(e^{\frac{v_D(t)}{\eta V_t}} - 1\right) \tag{1}$$

where I_s is the reverse-bias saturation current, η is the ideality factor, V_t is the thermal voltage, and $v_D(t)$ is given by the sum of the carrier (large signal) and the biological signal (small signal) $V_c\cos(\omega_c t) + V_n\cos(\omega_n t)$. The large-signal carrier excites the nonlinear diode, while the biological signal perturbs its I–V characteristics. The Taylor expansion of $i_D(t)$ [10] is defined as

$$\begin{aligned} i_D(t) = {} & \frac{1}{2}\alpha_2\left(V_c^2 + V_n^2\right) + \alpha_1 V_c\cos(\omega_c t) \\ & + \alpha_1 V_n\cos(\omega_n t) + \alpha_2 V_c V_n\cos\left[(\omega_c \pm \omega_n)t\right] \\ & + \frac{1}{2}\alpha_2 V_c^2\cos(2\omega_c t) + \frac{1}{2}\alpha_2 V_n^2\cos(2\omega_n t) \end{aligned} \tag{2}$$

where α_1 is equal to $\frac{I_s}{\eta V_t}$ and α_2 is equal to $\frac{I_s}{(\eta V_t)^2}$ and depend on the diode characteristic. The Taylor expansion reveals the presence of intermodulation products $f_c \pm f_n$, demonstrating the theoretical possibility of upconverting to high-frequency the intrinsic low-frequency biological signal.

Three commercial off-the-shelf Schottky diodes (SMC 95SQ015, ST Microelectronics BAT46, Skyworks SMS7621-079LF) were used to experimentally validate the frequency translation of the biological signal.

The three diodes were first tested in dc to evaluate their I–V characteristics and to assess the diodes' nonlinearities.

Fig. 2(a) shows the experimental setup including a function generator (Keysight 33500B), a low-noise preamplifier (stanford research systems SR560), and a signal analyzer (Keysight PXA N9030A). A 1× phosphate-buffered saline (PBS) solution (Sigma-Aldrich) was used to mimic a biological environment. Aluminum foil electrodes were placed on the beaker walls to inject the carrier signal and simulate the biological signal Fig. 2(b). The electrodes' size was approximately 6 cm × 2 cm and they were placed at a distance of 6 cm. The diode was placed in the middle of the beaker to maximize the coupling with the electric field generated by the electrodes Fig. 2(b).

The test bench Fig. 2(c) was used to measure the power across the diode and evaluate the efficiency of the mixing product. Conversion loss (CL) is used to evaluate the performance of the proposed method by measuring the power lost due to upconversion. CL is defined as

$$\mathrm{CL} = |P_{fc\pm fn}, \mathrm{dBm} - P_{fn}, \mathrm{dBm}| \tag{3}$$

where $P_{fc\pm fn}$ is the power of intermodulation, and P_{fn} is the power of the emulated low-frequency biological signal (i.e., the neuron). To optimize the new measurement system, it is essential to minimize CL so as to minimize the power loss due to upconversion.

The signal generator was set to 20 V_{pp} at 10 kHz and 200 mV_{pp} at 630 Hz for the carrier and biosignal, respectively. The voltage across

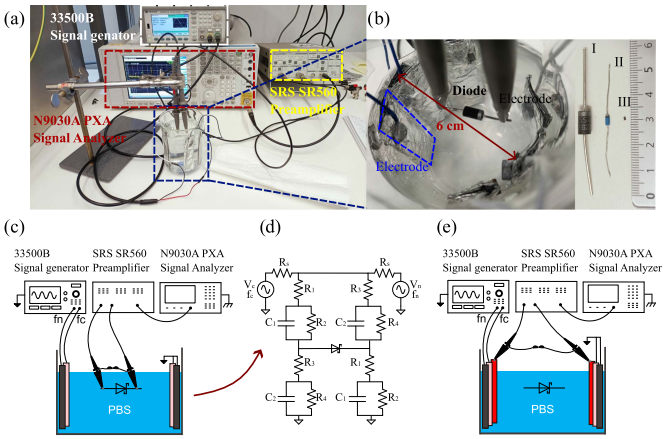

Fig. 2. (a) Experimental setup. (b) Magnification of beaker including aluminum electrodes immersed in PBS solution and the three Schottky diodes: 95SQ015 (I), BAT46 (II), and SMS7621-079LF (III). (c) Test bench for measuring the potential difference across the Schottky diodes in the PBS solution. (d) Equivalent electric model for the potential difference across the diode. (e) Test bench for measuring the propagation of the intermodulation signal in the PBS solution.

the diode terminal is acquired using differential low-noise preamplifier, configured with a bandwidth of 10 Hz–300 kHz and a gain of 1. The 50 Ω output of the preamplifier was connected to the PXA signal analyzer input (noise floor of −110 dBm). The peak-to-peak voltage (V_{pp}) is derived as

$$V_{pp} = \sqrt{10^{-3-\frac{-P_{dBm}}{10}}8R} \tag{4}$$

where P_{dBm} is the measured power, and R is the 50 Ω input impedance of PXA. The differential preamplifier is fundamental, allowing the diode decoupling from the 50 Ω impedance of the PXA [11]. The test was performed on all three diodes by varying the length of the diode terminals (2 cm, 1 cm, 0.5 cm, 0.1 cm). The length of the diode terminals changes the exposed area and the distance between the probes, thus varying the diode coupling with the signal generator. Electrochemical impedance spectroscopy (EIS) is a technique to measure the impedance of a system using a sinusoidal signal (e.g., ac voltage) over a wide range of frequencies. EIS was performed with a potentiostat (Metrohm Autolab PGSTAT302N) in the frequency range 0.1 Hz–100 kHz and an equivalent electrical model of the electrodes/PBS interfaces was derived Fig. 2(d).

The test bench Fig. 2(e) evaluated signal attenuation from the diode to the recording electrodes. The diode with the best nonlinearity was immersed in the solution, with recording probes connected to two other electrodes [red in Fig. 2(b)]. The diode terminal length was varied from 0.5 to 2 cm with a step of 0.5 cm, with carrier frequencies of 1 kHz, 3 kHz, 10 kHz, and 100 kHz.

III. RESULTS AND DISCUSSION

Fig. 3(a) shows the I–V curve of the diodes (95SQ015 in blue, BAT46 in yellow, SMS7621-079LF in green), highlighting their nonlinear properties. The ideality factor η of the diode is related to the slope of the $\frac{\log(i_D)}{v_D}$ curve, and it is derived by fitting the experimental data. The diode 95SQ015 (blue) shows the lowest η equal to 1.04, while the diode BAT46 and SMS7621-079LF (yellow and green) show higher η values equal to 1.30 and 1.29. The ideality factor of a Schottky diode is crucial for the mixer performance; a value close to 1 guarantees better

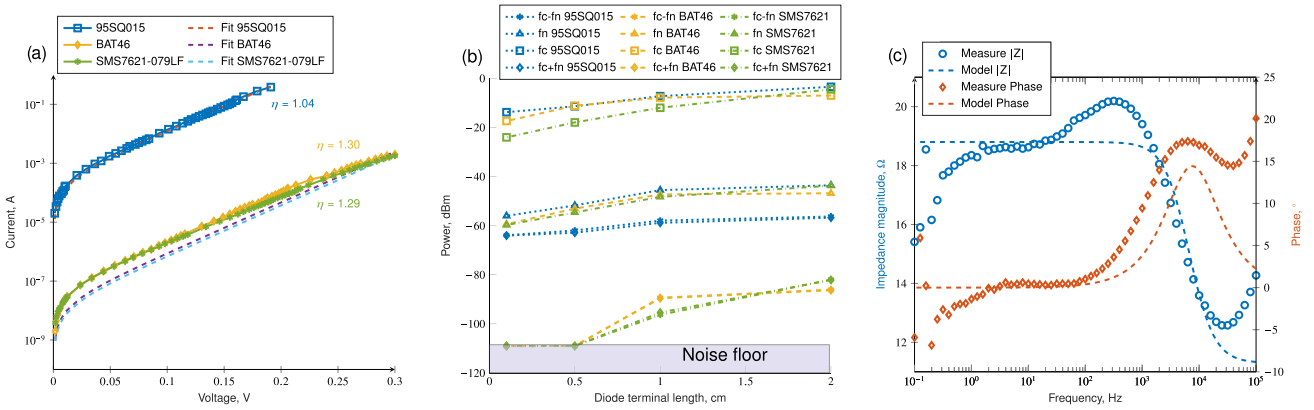

Fig. 3. (a) I–V curve of Schottky diodes. (b) Measurement of power at the ends of the three Schottky diodes Fig. 2(c) for 10 kHz carrier frequency (f_c), 630 Hz neuron frequency (f_n), and intermodulation product frequency ($f_c \pm f_n$). Four diode terminal lengths were tested. EIS measurement showing the electrode/PBS magnitude and phase impedance with the corresponding equivalent electrical model (R_1, R_2, and C_1) .

Table 1. Simulation and Measurement Results Obtain From Electrical Model Fig. 2(d) and the Test Bench Fig. 2(c)

Diode	P, dBm @f_c	P, dBm @f_n	P, dBm @$f_c \pm f_n$	CL, dB	Type
95SQ015	−3.42	−43.52	−56.24	12.72	Meas.
95SQ015[#]	−3.96	−43.80	−50.23	6.43	Sim.
BAT46	−6.96	−46.79	−86.06	39.27	Meas.
BAT46[†]	−7.07	−47.27	−81.06	33.79	Sim.
SMS7621-079LF	−4.43	−43.69	−82.12	38.43	Meas.
SMS7621-079LF[‡]	−4.03	−44.01	−84.45	40.44	Sim.

Electrical model:
[#] R_1 = 11.3 Ω, R_2 = 7.5 Ω, C_1 = 3.6 µF, R_3 = 22.9 Ω, R_4 = 20.4 Ω, C_2 = 5.60 µF
[†] R_1 = 20 Ω, R_2 = 33.2 Ω, C_1 = 4.44 µF, R_3 = 25.4 Ω, R_4 = 20 Ω, C_2 = 4.74 µF
[‡] R_1 = 11 Ω, R_2 = 7.5 Ω, C_1 = 3.6 µF, R_3 = 35 Ω, R_4 = 20.4 Ω, C_2 = 5.60 µF
Length of diode terminal 2 cm, V_c = 20V_{pp} , f_c = 10kHz, V_n = 200mV_{pp} , and f_n = 630Hz.

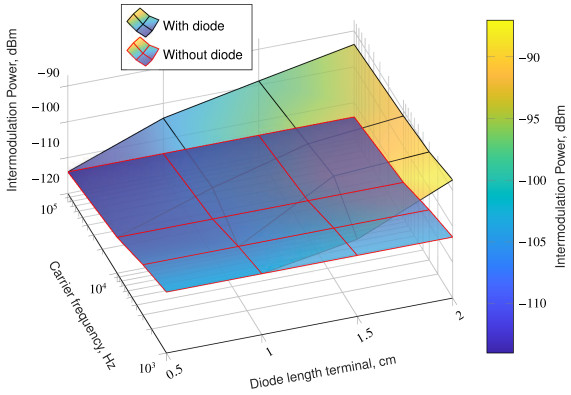

Fig. 4. Intermodulation power is measured in the PBS solution Fig. 2(e) with and without the 95SQ015 Schottky diode immersed in it at varying the carrier frequency and terminal length of the diode.

efficiency and lower CL. The 95SQ015 diode shows a low η, and thus, by (2) guarantees higher intermodulation than the other two diodes.

Fig. 3(b) shows the power across the diodes as a function of the diode terminal length. The plot includes the powers of the carrier signal (fc, squares), the simulated biological signal (fn, triangles), and the intermodulations products (fc-fn, asterisks) and ($fc + fn$, diamonds). While varying the diodes' terminal lengths, the power associated with the 20 V_{pp} carrier signal ranges from −13.76 to −3.42 dBm for the diode 95SQ015 (blue), from −17.35 to −6.96 dBm for BAT46 (yellow) and −24.02 to −4.43 dBm for SMS7621-079LF (green), ensuring sufficient power for all three diodes to reach the region of nonlinearity. Emulating the biological signal with a constant 200 mV_{pp} excitation, the corresponding power as a function of the diodes' terminal length ranges from −55.99 to −43.54 dBm for 95SQ015, from −59.37 to −43.69 dBm for BAT46, and −59.72 to −46.79 dBm for SMS7621-079LF. Powers in these ranges mean reproducing a biological signal with a voltage amplitude in the range of 653 μV_{pp} to 4.20 mV_{pp}. By shortening the length of the terminals, as expected, the coupling of the diode with the electric field decreases. The intermodulation products $f_c \pm f_n$ exhibit no differences across all tested diodes, indicating that both convey identical information. For the diode 95SQ015, the intermodulation products ($f_c \pm f_n$) are all above the noise floor, with amplitudes ranging from −64.02 to −56.24 dBm, showing an average CL relative to the biological signal of 11.11dB. For diodes BAT46 and SMS7621-079LF, only the intermodulation measurements with a terminal length greater than or equal to 1 cm yielded results above the noise floor. These measurements ranged from −96.32 to −81.94 dBm and −89.55 to −86.04 dBm, respectively. The average CL for BAT46 is 40.77 dB and for SMS7621-079LF is 42.95 dB. In summary, the results show that the diode 95SQ015 ensures superior performance compared to the other two diodes.

Table 1 compares the measured power using diodes with a terminal length of 2 cm with the simulated powers using the EIS-derived electrical equivalent model Fig. 2(d). Equivalent impedances were derived from the magnitude and phase obtained from the EIS analysis, as shown in Fig. 3(c). The values of all the parameters of the three electrical equivalent models are reported at the bottom of Table 1. Simulation and measurements match almost perfectly for both the carrier and the biological signal powers. Instead, the intermodulation products show discrepancies of 6.01 dB, 5.00 dB, and 2.33 dB, respectively, for diodes 95SQ015, BAT46, and SMS7621-079LF. The results obtained from the model simulations show a better CL than the measurements, most probably because the instrumentation and probes in the model were considered ideal. However, the electrical model shows the same trend as the experimental measurements, demonstrating and validating that the diode 95SQ015 has a better nonlinear effect, thus ensuring more efficient frequency translation with lower CL.

Fig. 4 presents the experimental results from the setup in Fig. 2(e), showing the measured intermodulation power in the PBS solution with and without the diode. Without the diode, the measurement is the noise floor. The intermodulation power was measured as a function of both the carrier frequency and the length of the diode terminals.

The latter significantly influences the amplitude of intermodulation, proportionally decreasing with the diode terminal's length due to reduced coupling with the recording electrodes. Instead, for a terminal length of 2 cm, the intermodulation power ranges from −93.77 to −87.04 dBm (above the noise floor) for all carrier frequency tested. For frequencies of 1 kHz and 3 kHz, the minimum length for acquisition above the noise floor is 1.5 cm (−98.29 dBm and −91.47 dBm, respectively). While for acquisitions at 10 kHz and 100 kHz, the signal can be measured even with a terminal length of 1 cm and it is equal to −101.29 dBm and −104.13 dBm, respectively. Intermodulation was observed within the solution despite significant distances between electrodes and diode terminals, demonstrating effective long-distance signal propagation. However, the signal is near the noise floor, which could potentially be reduced to −130 dB with advanced instrumentation. Extended terminals enhance coupling with electrodes, improving signal recording and propagation. Higher carrier frequencies provide advantages such as improved signal propagation through capacitive pathways and decreased noise floor.

Experimental tests demonstrated the feasibility of using a Schottky diode immersed in a solution to mix the biological signal and a high-frequency carrier, thus upconverting the information to a high-frequency band. This approach is promising for sensing applications, especially in fields demanding accurate measurement of low-frequency, low-amplitude signals. Differently, from [12], which used active electronics for signal upconversion after the acquisition, our method involves a diode in the solution for upconversion downstream in the acquisition chain. Although the effect of the passive diode mixer introduces a CL, the translation in frequency ensures a decrease in impedance by 2–3 orders of magnitude [8]. In addition, it has been demonstrated that the spectral density due to microelectrodes is above 100 $\mathrm{nV}/\sqrt{\mathrm{Hz}}$ at low frequency (i.e., Hz), while it is below 10 $\mathrm{nV}/\sqrt{\mathrm{Hz}}$ at higher frequency (i.e., kHz), thus providing better SNR [13]. Considering the best CL obtained of 11.11 dB and the noise spectrum in a 1 kHz band, an SNR improvement of 8.99 dB is estimated compared with the classical methodology for neural recording. An improvement in SNR of only 2.2 dB by optimizing the electrodes is reported in [14]. The simulated noise density due to the 95SQ015 diode is 60 $\mathrm{pV}/\sqrt{\mathrm{Hz}}$, thus being negligible.

Future work involves optimizing the proposed system using fully custom diodes to reduce CL and improve efficiency. A more realistic test bench, immersing only the terminals in the solution, will prevent interference with cell cultures, following an approach similar to that used with microelectrode arrays. An acquisition chain will be developed for high-frequency signals using an LNA with a bandpass filter for intermodulation acquisition (a lock-in amplifier may be used in noisy environments). In addition, integrating the external carrier signal generator and readout circuit into a single chip will greatly help to minimize the overall system as well. Finally, evaluating the impact of multiple diodes will pave the way for assessing the effectiveness and efficiency of a multichannel system. This approach promises to advance biological signal acquisition, opening the door for more effective signal acquisition solutions in biomedical research.

IV. CONCLUSION

This letter tested the feasibility of using a Schottky diode immersed in a solution to convert the low-frequency information of biological signals to a high-frequency band. Experimental tests revealed the necessary conditions to ensure a mixer's behavior of the Schottky diode, proving the concept. This method could enhance the acquisition of neural signals by improving the SNR and system reliability, making it suitable for miniaturized applications like sensor nodes for neural recording, both in vitro and in vivo.

ACKNOWLEDGMENT

This work was supported in part by the European CEREBRO Project under Grant 101046748 and in part by the Swiss SEFRI under Grant 22.00025.

REFERENCES

[1] C.-P. Segeritz and L. Vallier, "Chapter 9—cell culture: Growing cells as model systems in vitro," in *Basic Science Methods for Clinical*. M. Researchers, F. Y. Jalali Saldanha, and M. Jalali, Eds. Boston, MA, USA: Academic, 2017, pp. 151–172. [Online]. Available: https://www.sciencedirect.com/science/article/pii/B9780128030776000096

[2] E. Tibau, M. Valencia, and J. Soriano, "Identification of neuronal network properties from the spectral analysis of calcium imaging signals in neuronal cultures," *Front. Neural Circuits*, vol. 7, 2013, Art. no. 199. [Online]. Available: https://www.frontiersin.org/articles/10.3389/fncir.2013.00199

[3] N. Goshi, R. K. Morgan, P. J. Lein, and E. Seker, "A primary neural cell culture model to study neuron, astrocyte, and microglia interactions in neuroinflammation," *J. Neuroinflamm.*, vol. 17, 2020, Art. no. 155. [Online]. Available: https://doi.org/10.1186/s12974-020-01819-z

[4] R. Q. Quiroga and S. Panzeri, "Extracting information from neuronal populations: Information theory and decoding approaches," *Nature Rev. Neurosci.*, vol. 10, pp. 173–185, 2009. [Online]. Available: https://doi.org/10.1038/nrn2578

[5] F. H. Noshahr, M. Nabavi, and M. Sawan, "Multi-channel neural recording implants: A review," *Sensors*, vol. 20, 2020, Art. no. 904. [Online]. Available: https://api.semanticscholar.org/CorpusID:211086128

[6] L. Lyu, D. Ye, and C.-J. R. Shi, "A 340 nW/channel 110 dB PSRR neural recording analog front-end using replica-biasing LNA, level-shifter assisted PGA, and averaged LFP servo loop in 65 nm CMOS," *IEEE Trans. Biomed. Circuits Syst.*, vol. 14, no. 4, pp. 811–824, Aug. 2020.

[7] S.-I. Chang, S.-Y. Park, and E. Yoon, "Low-power low-noise pseudo-open-loop preamplifier for neural interfaces," *IEEE Sensors J.*, vol. 17, no. 15, pp. 4843–4852, Aug. 2017.

[8] A. Wang, D. Jung, D. Lee, and H. Wang, "Impedance characterization and modeling of subcellular to micro-sized electrodes with varying materials and PEDOT:PSS coating for bioelectrical interfaces," *ACS Appl. Electron. Mater.*, vol. 3, no. 12, pp. 5226–5239, 2021. [Online]. Available: https://doi.org/10.1021/acsaelm.1c00687

[9] A. Bagheri, M. T. Salam, J. L. Perez Velazquez, and R. Genov, "Low-frequency noise and offset rejection in dc-coupled neural amplifiers: A review and digitally-assisted design tutorial," *IEEE Trans. Biomed. Circuits Syst.*, vol. 11, no. 1, pp. 161–176, Feb. 2017.

[10] S. C. Bera, *Microwave Frequency Mixers*. Singapore: Springer, 2019, pp. 555–581. [Online]. Available: https://doi.org/10.1007/978-981-13-3004-9_18

[11] M. A. Callejón, J. Reina-Tosina, D. Naranjo-Hernández, and L. M. Roa, "Measurement issues in galvanic intrabody communication: Influence of experimental setup," *IEEE Trans. Biomed. Eng.*, vol. 62, no. 11, pp. 2724–2732, Nov. 2015.

[12] E. Kampianakis and M. S. Reynolds, "A biosignal analog front-end leveraging frequency translation," in *Proc. IEEE Sensors*, 2017, pp. 1–3.

[13] H. Steins et al., "A flexible protruding microelectrode array for neural interfacing in bioelectronic medicine," *Microsyst. Nanoeng.*, vol. 8, no. 1, Dec. 2022, Art. no. 131.

[14] R. Atmaramani et al., "Ruthenium oxide based microelectrode arrays for in vitro and in vivo neural recording and stimulation," *Acta Biomaterialia*, vol. 101, pp. 565–574, 2020. [Online]. Available: https://www.sciencedirect.com/science/article/pii/S1742706119307196

Open Access funding provided by 'Politecnico di Torino' within the CRUI CARE Agreement